Appl Phys B (2009) 96: 757–761
DOI 10.1007/s00340-009-3548-2

Applied Physics B
Lasers and Optics

Characterization of a MEMS-based pulse-shaping device in the deep ultraviolet

A. Rondi · J. Extermann · L. Bonacina · S.M. Weber · J.-P. Wolf

Received: 28 January 2009 / Revised version: 1 April 2009 / Published online: 2 May 2009

Abstract We describe the implementation and characterization of a micro-mirror-array set-up based on Micro-Electro-Mechanical System (MEMS) technology for femtosecond pulse shaping in the deep UV. We demonstrate its capability of re-compressing spectrally broadened UV pulses with a closed-loop approach based on a genetic algorithm. A single-shot synchronization scheme, taking advantage of the limited duty cycle of the device and allowing on-line correction of the signal, is described. The second dimension of the MEMS chip can be used to partially reduce the spatial chirp of the beam.

PACS 37.10.Jk · 07.10.Cm · 33.20.Lg

1 Introduction

The widespread success of coherent control techniques has recently induced considerable interest in the development of novel femtosecond pulse-shaping technologies. Among them, capabilities of shaping spectral phase, amplitude and polarization have been demonstrated [1, 2]. Most of these techniques rely on the use of 1D or 2D spatial light modulators (SLM) based on liquid crystal (LC) arrays. Despite some promising results in the UV [3], LC modulators are limited to the visible and NIR, while most important applications of coherent control in organic chemistry and biology require excitation in the UV. For instance, absorption bands of amino acids, proteins and nucleic acids in DNA–RNA all lie in the 200–300 nm region. Recent approaches for direct femtosecond pulse shaping in the near UV made use of acousto-optic [4–6], while indirect schemes are essentially based on frequency mixing of shaped pulses in the visible and NIR [7, 8]. Although encouraging, these techniques still suffer either of low throughput (some percent) due to diffraction losses or of insufficient spectral bandwidth (typ. 10% of the central wavelength). Group velocity dispersion in the crystal usually further reduces the flexibility of the output waveforms.

Considering the broad absorption features of organic molecules in solution and the fast decoherence time of their vibronic excitations, it is highly desirable to have at disposal an UV pulse shaper with no strict bandwidth limitations, based for instance on reflective elements, such as deformable mirrors [9] or MEMS micro-mirror arrays. While plain deformable mirrors usually lack in spectral resolution, MEMS appear as an appealing solution for these requirements. With their pioneering work, Hacker et al. demonstrated the aptness of a 2D MEMS device from Fraunhofer IPMS for pulse-shaping applications at 400 nm [10]. Several groups successively exploited the 2D features of the same MEMS chip for shaping NIR pulses in diffraction mode [11], as well as for shaping two beams (NIR and UV–VIS) simultaneously [12].

Here, we report on the development of a MEMS-based custom design for broadband femtosecond pulse shaping in the deeper UV at around 266 nm. In the following, we characterize the device in this wavelength region, address a series of technical details related to its operation and demonstrate its capability of re-compressing self-phase modulation (SPM) broadened UV pulses with a closed-loop approach based on a genetic algorithm.

A. Rondi · J. Extermann · L. Bonacina (✉) · S.M. Weber · J.-P. Wolf
Université de Genève, GAP-Biophotonics, 20 Rue de l'Ecole de Médecine, 1211 Geneva 4, Switzerland
e-mail: luigi.bonacina@unige.ch

2 Experimental details

2.1 Optical set-up

The output of a 1 kHz amplified Ti:Sapphire laser system delivering 2 mJ pulses is first separated into two arms by a 50/50 pellicle beam splitter. The transmitted component is used to generate 266 nm (UV) light by an in-line frequency tripler. The position of the grating compressor of the amplifier is optimized to yield the most efficient conversion of the fundamental to the third harmonic. As shown in Fig. 1, the UV is then focused by a lens of 35 mm focal length onto a 3 mm thick CaF_2 plate to broaden it spectrally up to 10 nm at $1/e^2$. The broadened pulses are then re-collimated by a second 35 mm lens and sent into the all-reflective shaper apparatus (left of Fig. 1 and picture in Fig. 2). The shaper is based on a 1200 grooves/mm blazed grating and on a cylindrical mirror with focal length of 250 mm, which collimates the spectrum dispersed by the grating along the y axis onto the MEMS chip. The latter is protected by a window treated with a 250–440 nm UV anti-reflection coating. With these settings the device can theoretically access a maximal bandwidth of 40 nm at the Fourier plane, with a resolution of 0.13 nm/pixels and a corresponding temporal shaping window extending for ∼3.5 ps [13]. Note that even though the full bandwidth potential was not exploited in the following measurements, there are no device restrictions to access, for example, the UV portion of the extremely broad spectra generated by filamentation, recently reported in Refs. [14, 15]. Spectral phase-shifts are introduced by creating a striped pattern along the x axis by applying the same deflection to all the micro-mirrors belonging to the same line. The 800 nm pulses (IR) reflected off by the beam splitter are first temporally compressed down to 120 fs by a grating compressor and then focused together with the shaped UV onto a 200 µm thick BBO crystal to generate a difference frequency mixing (DFM) signal at 400 nm detected by a Si photodiode.

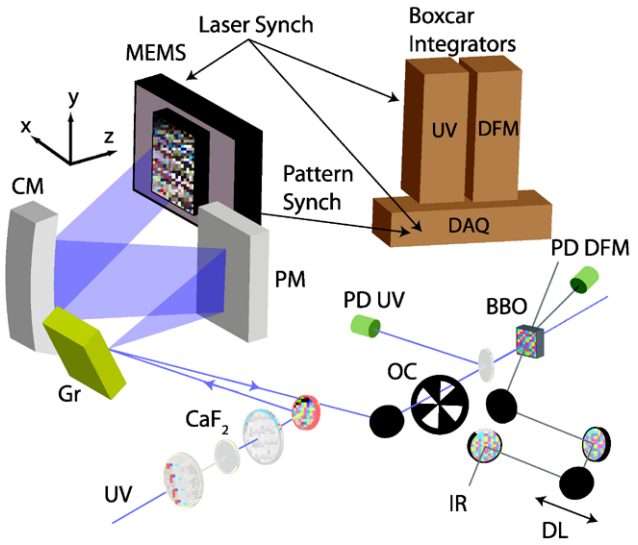

Fig. 1 Experimental scheme. Gr: grating; PM: plane mirror; CM: cylindrical mirror; DL: temporal delay line; OC: optical chopper. PD UV/DFM: detection photodiodes, DAQ: acquisition card. The OC is synchronized to half the repetition rate of the laser to reject every second UV pulse

2.2 MEMS chip and synchronization scheme

The main characteristics of the MEMS chip were reported in the previous paper by Hacker et al. [10]. Briefly, it consists of a rectangular array of 240 × 200 of 40 µm side pixels with fill factor of 81%. The maximum pixel stroke is 400 nm, i.e. $\sim 6\pi$ phase shift at 266 nm after shaper. The chip is attached directly on its 21 × 30 cm electronic driving board as shown in Fig. 2. Given the increasing interest shown by various research groups for this device—which was originally intended for wave-front correction and not for temporal pulse shaping [16]—we will describe in some details the issues related to its efficient addressing in combination with an amplified femtosecond laser system. A dedicated synchronization was developed to adapt the detection to the limited duty cycle of the MEMS shaper. According to its specifications, the MEMS chip can set a deflection pattern in 50 µs and

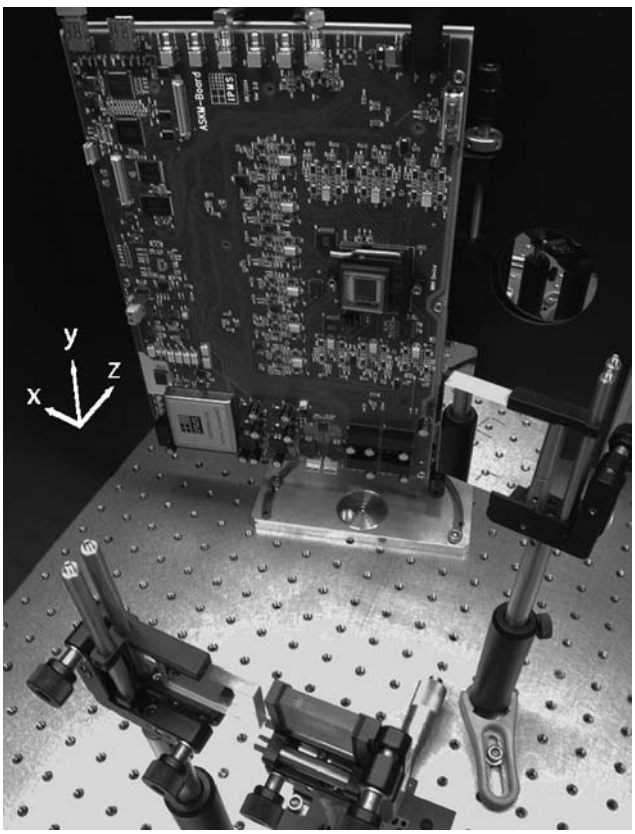

Fig. 2 Picture of the shaper set-up. We recognize the MEMS chip placed in the middle right of the driving board. The axes are equivalent to those in Fig. 1

successively maintain it for a period of τ_{ON} ranging from 100 µs to 1 s followed by an idle period of τ_{OFF} lasting at least $17 \times \tau_{ON}$. Normally, to minimize the idle time τ_{OFF}, the best approach would be to trigger externally the device and use the shortest possible τ_{ON}, so that an operation cycle is completed in 1.8 ms and every second pulse at kilohertz rate can be shaped. Unfortunately, we found out that even for τ_{ON} of the order of 100 µs the shortest idle time is $\tau_{OFF} > 3$ ms. Therefore, the settings used for the measurements presented in this paper correspond to $\tau_{ON} = 320$ µs, chosen to maximize the active shaping time window without reducing the most efficient exploitation of the device as compared to the kilohertz laser output. The signal detected during the τ_{OFF} period was used to record a running reference associated to the "flat" mask, corresponding to no deflection applied to the micro-mirrors. Note that, even if we were warned by the supplier that the τ_{OFF} period could be associated to a quasi-random pattern, we only noticed a minor and constant difference, of the order of 5%, between the signal intensities detected during τ_{OFF} and those measured with a flat pattern imposed. We decided therefore to take advantage of the idle period for recording a reference signal of the laser intensity.

Detection is based on a single-shot approach according to the following scheme: the pattern-ready synchronization signal from the MEMS device is used as principal trigger to start an acquisition cycle of N consecutive samples of four independent analog channels (UV and DFM intensity, chopper status [UV blocked or not] and MEMS device status [pattern applied or not]). The acquisition of each sample series is synchronized with the repetition rate of the laser system. At the end of the acquisition the driving software sorts the DFM and the UV signal shots according to their respective MEMS device status (pattern ON or OFF) and chopper status (UV pulse present on the BBO crystal or not) calculating the UV fluctuation-corrected DFM signal as:

$$\frac{I_{\mathrm{DFM}}(\mathrm{IR},\mathrm{UV})^{\mathrm{ON(OFF)}} - I_{\mathrm{DFM}}(\mathrm{IR})^{\mathrm{ON(OFF)}}}{I_{\mathrm{UV}}^{\mathrm{OFF}}}.$$

This approach enables performing a series of statistical checks on the signal noise allowing the rejection of isolated bad laser shots or correct for long-term laser drifts [17].

2.3 Technical remarks

We consider useful to report here three main drawbacks associated to the use of this device in the context of femtosecond pulse shaping:

1. A strong diffraction of the beam (Fig. 3), even though this effect is inherent to any pixellated device, which limits the actual $I_{\mathrm{out}}/I_{\mathrm{in}}$ throughput to 0.1. We also observed a dependence of the diffraction efficiency on the mask pattern applied, leading to a complex phase/amplitude coupling. In some cases, the relative amplitude of the shaped pulses (nominally phase-only) could be as low as 70% of the unshaped ones.
2. A long thermalization time (of the order of a few tens of minutes) after powering on of the device, which influences the relative time delay between the UV and the IR pulse.
3. When $\tau_{ON} > 1$ ms, we systematically remarked a variation of the optical signal over successive shots in the pulse train suggesting a change in the deflection pattern during long mask application (longer than a few ms).

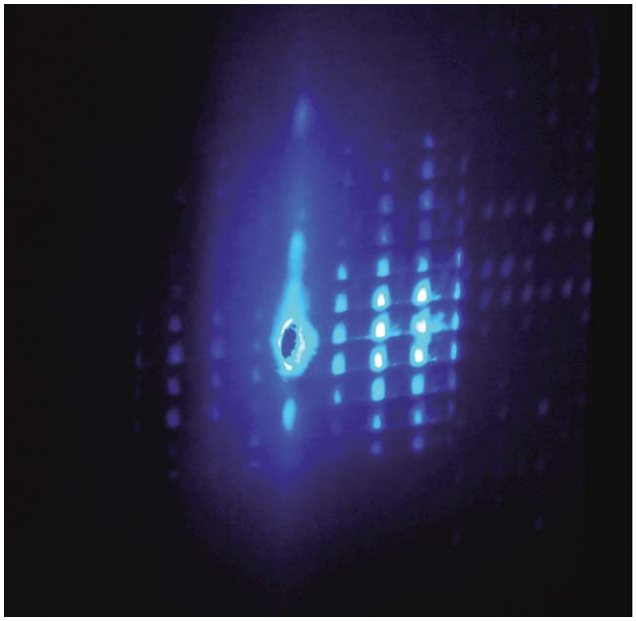

Fig. 3 Picture of the diffraction pattern created after reflection on the MEMS chip (*left*: hole for the incident beam; *right*: diffraction pattern). The reflected beam intensity in the zeroth order amounts to 10% of the incident beam intensity

3 Results

To complement the preceding work of Hacker et al. demonstrating the capability of the device to produce well-defined pulse shapes with calculated phase masks [10] during the present study, we exclusively focused our attention to a closed-loop approach, to verify the aptness of the device to perform long-term feedback-driven optimizations.

In Fig. 4 we summarize the results obtained by closed-loop optimizing the DFM signal with UV pulses of different characteristics impinging on the BBO crystal. The time resolution of the measurement is given by the independently measured IR autocorrelation (thick line in Figs. 4b and 4e) yielding 120 fs. The duration of the unshaped and not spectrally broadened UV, strongly chirped by the presence of

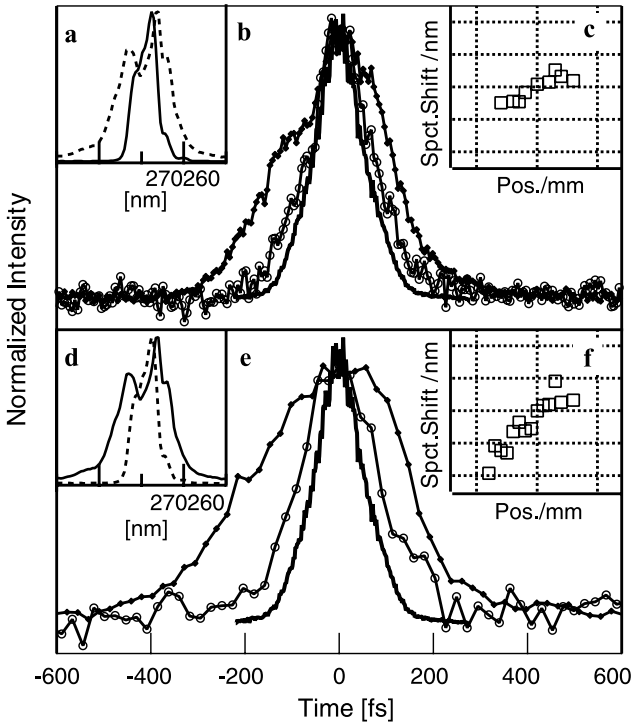

Fig. 4 Original (**a**) and SPM broadened (**d**) pulse spectra. IR autocorrelation (*thick line*), UV/IR cross-correlation for UV unshaped (*dots*) and shaped (*open circles*) pulses in the case of original (**b**) or broadened (**e**) spectra. First spectral moment shift at different positions within the beam profile for the original (**c**) and broadened (**f**) pulses. In panels (**c**) and (**f**) the horizontal grid lines are spaced by 1 mm and vertical grid lines by 1 nm

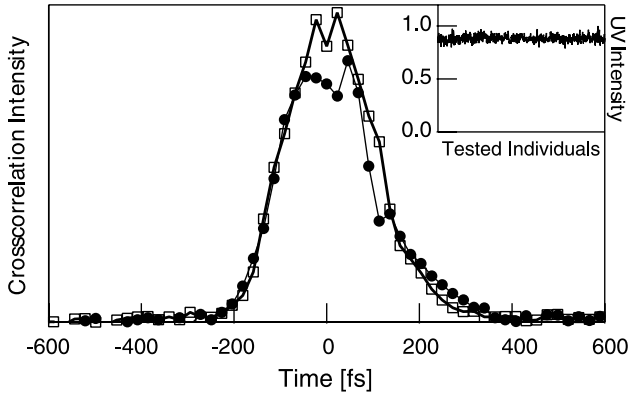

Fig. 5 UV/IR cross-correlation for 1D- (*dots*) and 2D-shaped (*open squares*) pulses in the case of a broadened spectrum. Assuming Gaussian pulse shapes, the 266 nm duration at FWHM is 115 fs for the 1D optimization and 104 fs for the 2D optimization. *Inset*: evolution of the shaped UV pulse intensity during the 2D optimization

4 mm of fused silica, clearly dominates the UV/IR cross-correlation in Fig. 4b (dots). When the shaping mask found for maximizing the DFM signal is applied to the UV, on the other hand, the UV/IR cross-correlation (open circles) results practically coincident with the IR autocorrelation, evidencing the shorting of the UV pulse which should now present a duration of the order of 100 fs.

For emphasizing the control possibilities on the ultrafast molecular dynamics of biological systems, we are interested in shaping UV pulses of wider bandwidth [18, 19]. Consequently we tested the shaping capability of the set-up on a non-linearly broadened spectrum. The insets (a) and (d) in Fig. 4 compare original and SPM broadened spectra, indicating an increase from 5 to 10 nm at $1/e^2$. The cross-correlation trace of the unshaped pulse in Fig. 4e indicates a significant increase of the UV pulse duration and a change in the overall shape of its time envelope. It is noteworthy to point out that masks based on chirp compression calculations cannot work effectively on such a peculiar pulse shape, and the closed-loop approach pursued here emerges as the most natural approach. Not surprisingly, the signal intensity fluctuations in the broadened case are stronger due to the highly non-linear interactions at the basis of the spectral broadening, and the correction of the DFM signal by $I_{\mathrm{UV}}^{\mathrm{OFF}}$ becomes essential for the optimization procedure. The latter is performed using the nonelitist genetic approach first developed by Deb [20] and more recently modified and adopted for pulse-shaping applications [21]. For the measurements presented, typically convergence was obtained after ∼60 generations with a population of 16 individuals. The final outcome shows a sensible decrease in pulse duration and a clear symmetrization of the temporal profile. However, the resulting trace remains longer than the IR autocorrelation. A possible reason justifying the diminished outcome of the optimization can be ascribed to the worsening of the spatial chirp as a consequence of the broadening mechanism [22], as evidenced by the plots in Figs. 4c and 4f, which report the shift of the first moment of a series of spectra sampled with a 50 μm fiber at different positions of the UV beam profile.

One can expect that, by taking advantage of the second dimension of the MEMS chip, this effect can be partially corrected. Thus, we proceeded in further optimizing the result of striped-pattern optimizations by lifting the constrain of equal deflection for all the micro-mirrors of a given line along x. In doing so we generally obtained a systematic increase of the shaped signal amplitude I_{DFM} of the order of 10–15%, which was accompanied by a very slight decrease of pulse duration, and only a limited improvement on the wings of the cross-correlation traces (Fig. 5). Interestingly, the increase of I_{DFM} was not associated to any augmentation of I_{UV} (inset of Fig. 5) ruling out the trivial explanation of this intensity increment as a diffraction-driven effect. We therefore ascribe these observations to the partial re-phasing of the spatial frequencies along x which, not being sustained by a similar correction along the y axis, determines only a small improvement of the temporal traces.

4 Conclusions

We have described the implementation of a reflective 2D-MEMS chip for direct broadband UV pulse shaping. We demonstrated here that with a proper synchronization scheme the drawbacks of a limited duty cycle can be greatly reduced allowing an efficient addressing of the device with a kilohertz system. This way, we realized the temporal pulse compression of both a narrow and a spectrally broadened pulse. In the former case only one dimension of the MEMS mask is independently addressed, in the second case, for partially reducing the effect of the spatial chirp, both dimensions can be kept independently active. Among the different pulse-shaping techniques, MEMS-based devices present clear advantages in terms of wavelength and bandwidth flexibility. On the other hand, the strong diffraction inherent to the pixellated nature of the device should be taken into account because it results the principal factor at the origin of the low optical throughput of the set-up.

Acknowledgements We are grateful to M. Moret, B. Thuillier and V. Boutou for their contribution in the design of the shaper. We acknowledge the support of the Swiss National Science Foundation (CIBA project, contract No. 2000021-111688), the Swiss SER through the COST P18 project and the Swiss NCCR QP project.

References

1. T. Brixner, G. Gerber, Femtosecond polarization pulse shaping. Opt. Lett. **26**, 557–559 (2001)
2. M. Ninck, A. Galler, T. Feurer, T. Brixner, Programmable common-path vector field synthesizer for femtosecond pulses. Opt. Lett. **32**, 3379–3381 (2007)
3. K. Hazu, T. Sekikawa, M. Yamashita, Spatial light modulator with an over-two-octave bandwidth from ultraviolet to near infrared. Opt. Lett. **32**, 3318–3320 (2007)
4. M. Roth, M. Mehendale, A. Bartelt, H. Rabitz, Acousto-optical shaping of ultraviolet femtosecond pulses. Appl. Phys. B, Lasers Opt. **80**, 441–444 (2005)
5. S. Coudreau, D. Kaplan, P. Tournois, Ultraviolet acousto-optic programmable dispersive filter laser pulse shaping in KDP. Opt. Lett. **31**, 1899–1901 (2006)
6. B.J. Pearson, T.C. Weinacht, Shaped ultrafast laser pulses in the deep ultraviolet. Opt. Express **15**, 4385–4388 (2007)
7. C. Schriever, S. Lochbrunner, M. Optiz, E. Riedle, 19 fs shaped ultraviolet pulses. Opt. Lett. **31**, 543–545 (2006)
8. P. Nuernberger, G. Vogt, R. Selle, S. Fechner, T. Brixner, G. Gerber, Generation of shaped ultraviolet pulses at the third harmonic of titanium-sapphire femtosecond laser radiation. Appl. Phys. B, Lasers Opt. **88**, 519–526 (2007)
9. E. Zeek, K. Maginnis, S. Backus, U. Russek, M. Murnane, G. Mourou, H. Kapteyn, G. Vdovin, Pulse compression by use of deformable mirrors. Opt. Lett. **24**, 493–495 (1999)
10. M. Hacker, G. Stobrawa, R. Sauerbrey, T. Buckup, M. Motzkus, M. Wildenhain, A. Gehner, Micromirror SLM for femtosecond pulse shaping in the ultraviolet. Appl. Phys. B, Lasers Opt. **76**, 711–714 (2003)
11. K.W. Stone, M.T.W. Milder, J.C. Vaughan, K.A. Nelson, Spatiotemporal femtosecond pulse shaping using a MEMS-based micromirror SLM. Ultrafast Phenom. XV **88**, 184–186 (2007)
12. T. Abe, G. Wang, F. Kannari, Femtosecond pulse shaping on two-color laser superposition pulse using a MEMS micromirror SLM. 2008 Conference on Lasers and Electro-Optics & Quantum Electronics and Laser Science Conference, vols. 1–9 (2008), pp. 2832–2833
13. A.M. Weiner, Femtosecond pulse shaping using spatial light modulators. Rev. Sci. Instrum. **71**, 1929–1960 (2000)
14. S.A. Trushin, S. Panja, K. Kosma, W.E. Schmid, W. Fuss, Supercontinuum extending from >1000 to 250 nm, generated by focusing ten-fs laser pulses at 805 nm into Ar. Appl. Phys. B, Lasers Opt. **80**, 399–403 (2005)
15. C.P. Hauri, L.T. Vuong, A.L. Gaeta, Optimized supercontinuum generation and pulse self-compression in filaments from the UV to the IR. 2008 Conference on Lasers and Electro-Optics & Quantum Electronics and Laser Science Conference, vols. 1–9 (2008), pp. 1855–1856
16. A. Gehner, W. Doleschal, A. Elgner, R. Kauert, D. Kunze, N. Wildenhain, Active-matrix addressed micromirror array for wavefront correction in adaptive optics. MOEMS Miniaturized Syst. II **4561**, 265–275 (2001)
17. M. Roth, J. Roslund, H. Rabitz, Assessing and managing laser system stability for quantum control experiments. Rev. Sci. Instrum. **77**, 083107 (2006)
18. B.Q. Li, H. Rabitz, J.P. Wolf, Optimal dynamic discrimination of similar quantum systems with time series data. J. Chem. Phys. **122**, 154103 (2005)
19. E.C. Carroll, A.C. Florean, P.H. Bucksbaum, K.G. Spears, R.J. Sension, Phase control of the competition between electronic transitions in a solvated laser dye. Chem. Phys. **350**, 75–86 (2008)
20. K. Deb, A. Pratap, S. Agarwal, T. Meyarivan, A fast and elitist multiobjective genetic algorithm: NSGA-II. IEEE Trans. Evol. Comput. **6**, 182–197 (2002)
21. L. Bonacina, J. Extermann, A. Rondi, V. Boutou, J.P. Wolf, Multiobjective genetic approach for optimal control of photoinduced processes. Phys. Rev. A **76**, 023408 (2007)
22. X. Gu, S. Akturk, R. Trebino, Spatial chirp in ultrafast optics. Opt. Commun. **242**, 599–604 (2004)